energies

MDPI

Article

Efficient Output Photovoltaic Power Prediction Based on MPPT Fuzzy Logic Technique and Solar Spatio-Temporal Forecasting Approach in a Tropical Insular Region

Fateh Mehazzem *, Maina André and Rudy Calif

Univ Antilles, LaRGE Laboratoire de Recherche en Géosciences et Energies (EA 4539),
F-97100 Pointe-à-Pitre, France
* Correspondence: fateh.mehazzem@univ-antilles.fr

Abstract: Photovoltaic (PV) energy source generation is becoming more and more common with a higher penetration level in the smart grid because of PV energy's falling production costs. PV energy is intermittent and uncertain due to its dependence on irradiance. To overcome these drawbacks, and to guarantee better smart grid energy management, we need to deal with PV power prediction. The work presented in this paper concerns the study of the performance of the fuzzy MPPT approach to extract a maximum of power from solar panels, associated with PV power estimation based on short time scale irradiance forecasting. It is particularly applied to a case study of a tropical insular region, considering extreme climatic variability. To validate our study with real solar data, measured and predicted irradiance profiles are used to feed the PV system, based on solar forecasting in a tropical insular context. For that, a spatio-temporal autoregressive model (STVAR) is applied. The measurements are collected at three sites located on Guadeloupe island. The high variability of the tropical irradiance profile allows us to test the robustness and stability of the used MPPT algorithms. Solar forecasting associated with the fuzzy MPPT technique allows us to estimate in advance the produced PV power, which is essential for optimal energy management in the case of smart energy production systems. Simulation of the proposed solution is validated under Matlab/Simulink software. The results clearly demonstrate that the proposed solution provides good PV power prediction and better optimization performance: a fast, dynamic response and stable static power output, even when irradiation is rapidly changing.

Keywords: boost converter; MPPT fuzzy; output PV power estimation; PV system; solar forecasting; STVAR model; tropical insular region

1. Introduction

Solar energy prevision helps to reduce grid imbalance charges and avoid penalties. Thus, the forecast for the operation of solar power plants gives visibility as to the resources that will be available in the coming minutes, hours, and days. Integrating forecasting into the production process helps operators to limit the uncertainty associated with photovoltaic energy production. As a result, this allows a massive and secure injection of solar energy into the grid.

In a tropical insular context, for which the costs of supplying electricity are higher than those of the rest of the world, the challenges induced by a massive development of electrical renewable energies for supply–demand balance and network stability are indeed particularly important [1]. Wind and solar energy are the most promising renewable energy resources because of their potential and availability. In the last decades, PV systems have become more and more common in electricity generation due to their: price reduction, efficiency, and increased life. In addition, they provide clean and sustainable energy. The overall output power of different PV systems can vary under dynamic irradiance fluctuations [2].

Nowadays, the rapid growth of the penetration of renewable energy sources into distribution grids brings new challenges to overcome: stability, cost system operation, and congestion management. An effective weather forecasting based on a great spatial resolution, and the integration of artificial intelligence, contribute to obtaining an improved state estimation of the power system and avoid it reaching a dangerous state [3,4].

The privileged location of the tropical insular regions, which have particularly favorable climatic conditions with more than 1400 h of insolation per year, is a major advantage for photovoltaic solar production. On the other hand, these regions are characterized by high variability of observed irradiance [5]. This high variability is the consequence of a solar microclimate's diversity due to its complex topography in a small space (mountainous/low orography, land/sea contrasts) and frequent cloud formation in the tropical zone [6–9]. In [5,9–11], the types of days and the fluctuating nature of solar radiation from Guadeloupe island (the island of our measurements sites) are highlighted, exhibiting regimes of variability. Moreover, these islands are not electrically interconnected, which makes their network fragile, and it requires a threshold for the power instantly consumed from intermittent renewable energies (solar and wind) to be set.

In the literature, several metrics have been defined for the variability quantification of irradiance. A few metrics can be quoted such as the variability index (VI) [12], which is a ratio including measured irradiance, clear sky irradiance signal, the number of consecutive observations, and the averaging interval of the time series. In [12], the author showed a classification of sites and periods of time when variability is significant. In [13], the intra-hour variability score (IHVS) [13] captures several key variability characteristics into a single metric for irradiance, or PV output power, data. It is shown that this metric facilitates the comparison of the variability of PV systems of different sizes, with different configurations, across different climates. In [14], the daily aggregate ramp rate (DARR) represents the sum of all absolute increment values during a given hour or day. This metric made it possible to characterize variability due to geographical dispersion by simulating a step-by-step increase in the plant size at the same location. In [15], the variability score (VS) is based on increments in temporally averaged data, with averaging time scale, expressed in a percentage. In [16], the nominal variability is defined as the ramp rate's variance of clear sky index. This metric can clearly distinguish two extremum cases of insolation conditions, namely, perfectly clear conditions (i.e., no variability) and heavily overcast conditions. In [17], the variability score VS, defined as the maximum value of ramp rate magnitude (RR0) times ramp rate probability, has been performed on the same measurements site under our study to categorize typical days as a function of their variability [11]. The study showed that 58% of ramp rates are higher than 50 W·m^{-2} concerning the intermittent cloudy sky days at 5 min time scales, and the type of days presenting the higher magnitude of ramp rate and higher VS values. Thirty percent of such days occurred in the year 2012. Moreover, the results revealed that VS increased over Δt.

In this challenging context, the forecasting technique needs to have robustness and predictive efficiency allowing high variability to be forecast at short time scales. The high variability of irradiance leads to increased grid variability and uncertainty for grid-connected solar photovoltaics (PV) as penetration increases. The development of an efficient forecasting model contributes to better management by power system operators and/or PV plant owners.

In the recent literature, the spatial and temporal characteristics of irradiance are considered by introducing the information observed at several neighboring locations. The spatio-temporal techniques have already shown an improvement in the forecast's quality [18–20] for several environmental processes: in wind velocity fields such as in [21] where neural and geostatistical techniques were developed to obtain the wind speed maps, or in [22] using a VAR (vector autoregressive) model to forecast wind speed and atmospheric concentration of carbon monoxide by integrating spatio-temporal parameters from spatially sparse sites. In [23], the authors developed Taylor kriging technics also applied to wind speed forecasting and improving the predictive performance compared to the ARIMA (au-

toregressive integrated moving average) model, and other techniques for modeling wind speed such as space–time covariance models were described and applied in [24]. In the solar forecasting area, several spatio-temporal tools have been developed such as kriging approaches: cross-validation with spatial kriging integrating parameters of cloud motion in [25] resulting in a detailed map of solar radiation, or space–time kriging to forecast irradiance at arbitrary spatial locations, such as in [26] with a variance–covariance structure explored and defined, in [27] integrating shrinkage parameters, or in [28] to forecast very short-term irradiance at unobserved locations. Moreover, other approaches have been developed in the literature such as lasso-based variable selection [29], spatio-temporal ARMA (autoregressive moving average) such as (STARMA) models ([30,31], or spatio-temporal vector autoregressive (STVAR) models [6,27] providing future irradiance based on a linear combination of past observations at the most relevant neighboring locations.

PV power production is considered a nonlinear probabilistic process because it is affected by the variation in:

- many weather parameters such as solar irradiance, temperature, wind, etc.;
- the PV cells nonlinear model;
- the DC-DC converter model;
- outages of the grid and possible islanding conditions of the PV parks;
- other operation conditions.

The output power of the PV system changes with time and depends on the variability of meteorological factors. Accurate PV power forecasting contributes to improving the stability, security, and reliability of grid operation, as well as scheduling and grid energy management [32]. It also affects power quality, voltage surges, reverse power flows, etc. PV power forecasting can be performed for different forecast time horizons, from very short time scales (minutes) to long time scales (days). The choice of forecast time horizon depends mainly on applications [33]. PV power forecasting for the short-term horizon is used, for example, in PV power ramp rate estimation [34]. Fast irradiance fluctuations affect the quality and reliability of PV power. PV power forecasting for the long-term horizon is used, for example, in energy management optimization in microgrids [35].

PV power forecasting methods can be classified into two categories: direct and indirect methods [36]. Direct methods consist of applying physical, statistical, artificial intelligence, or hybrid models to PV measurements. They propose several techniques and models. Among them are: Physical models, obtained from the modeling of solar radiation dynamics in the atmosphere using physics laws, which is more efficient in long-term prediction [37]. Statistical approaches that use historical data samples and give better performance in short-term prediction [38]. Artificial intelligence approaches, also known as machine learning approaches. They use different architectures of artificial neural network (ANN) and fuzzy techniques. They are based on basic operations of training and testing. Their advantage is that they deal with complex nonlinear features effectively, and their main drawback is the requirement for a large quantity of data during the training stage [39]. Deep learning structures are more popular nowadays [40]. Hybrid approaches, which are a combination of two or more approaches that give more accuracy in PV power forecasting in different cases [41].

Indirect methods consist of fragmenting the power prediction problem into two stages: forecasting weather parameters and introducing them in commercial PV simulation software to forecast the PV power generation. Solar forecasting was conducted for different time scale horizons and using different forecasting methods cited above.

Concerning PV power short-term horizon forecasting applications, other approaches are proposed in the literature to estimate the expected power of a PV system from a ramp rate characterization. An analysis of variability is therefore investigated, such as in [42], exhibiting the frequency of a given fluctuation from output PV power for a certain day by an analytic model, and [43] who demonstrated the smoothing of rapid ramps observed in a location point by large PV plants, which was strengthened in [16] by the result of the aggregation of multiple PV plants. In [14], a quantitative metric called the daily aggregate

ramp rate (DARR) was proposed to quantify, categorize, and compare daily variability from power output, across multiple sites. In [16], models were developed exhibiting a capacity to extrapolate the resulting variability on an ensemble of power plants, and, in [34], a method was proposed to estimate the largest expected PV power ramp rates (RR).

The works in the literature clearly show the purposes of power forecasting, namely, the development of strategies to mitigate the impact of solar variability on electric power grids, the optimization of the design and size of PV power plants, and, consequently, a maximization of their effectiveness and minimization of costs by using the curve fitted to the largest RR ratios, irradiance, and cloud shadow velocities dataset. In [44], the authors propose the implementation of an optimized solar PV utilization using a low-cost hardware platform to improve efficiency, and for better saving of the grid energy. The proposed solution is based on an online intelligent algorithm.

As a reminder, in a photovoltaic system, the maximum power point (MPP) corresponds to the point of tangency between the characteristic points of the photovoltaic generator for a certain value of solar radiation [45]. The role of the MPPT is to precisely detect at every moment this point of maximum energy efficiency. The performance of an MPPT controller depends on how quickly it reaches the point of maximum power, how it oscillates around that point, and how robust it is in the face of abrupt atmospheric changes. Several power point maximum (PPM) tracking algorithms have been cited in the literature over the last few years [46–48]. These algorithms can be mainly classified as conventional, metaheuristic, artificial intelligence, nonlinear, and hybrid algorithms.

Conventional MPPT techniques such as Perturb and Observe (P&O) [49], Incremental Conductance (IC) [50], and Hill Climbing (HC) [51] give good results under uniform irradiance conditions. However, this performance is not guaranteed during transitional regimes. Other works are based on metaheuristic approaches such as particle swarm optimization (PSO) [52] and genetic algorithms (GA) [53]. Their performance depends on selected design parameters and initial conditions. MPPT techniques based on artificial intelligence such as fuzzy logic (FL) [54] and neural networks (NN) [55] have become more and more popular. They have the advantage of working even with imprecise input values and they do not need a high precision mathematical model. In addition, they can deal with nonlinearities. In recent years, many MPPT techniques based on nonlinear control have been proposed. Among them are sliding mode [56] and backstepping [57]. These approaches are known for their robustness and stability using Lyapunov functions. Hybrid MPPT techniques are a combination of two or more of the MPPT techniques cited before [58].

Fuzzy logic was developed by Zadeh in 1965 from his theory of fuzzy subsets [59]. It allows us to imitate human reasoning by using the different collected data in linguistic forms. One of the main interests of the use of fuzzy logic consists of being able to pass, simply through the intermediary of linguistic rules, the expertise that one may have of the process towards the controller. It is thus possible to transform the expert's knowledge into simple rules that the controller can implement. The ease of implementing solutions for complex problems is then associated with robustness for uncertainties and the possibility of integrating the expert's knowledge.

In MPP optimization problems of PV systems, it is recognized that classical methods [49–51] are widely used due to their simple structure and the fact that they require fewer measured parameters, but their speed of convergence is variable. In addition, the system will constantly oscillate around the MPP. These oscillations can be minimized by reducing the value of the increment step. However, a small increment value can slow down the search for the MPP. This drawback allowed us to find in permanence a compromise between precision and speed. In addition, it is an unsuitable method for rapidly changing weather conditions. Conversely, fuzzy MPPT controllers are well adapted to this type of problem and behave well in various atmospheric conditions. They converge quickly, although they can work with imprecise inputs, and do not require a well-known mathematical model [54,60,61]. Moreover, fuzzy control is known for its robustness and its adaptive

nature, giving it high performance with respect to parameter variation and disturbances of the system.

In these works, a structure with several steps is defined to feed our PV production system, firstly performing irradiance forecasting from a STVAR model. The model was developed in [4] and showed good predictive performance for time scales from 5 min to 1 h. This spatio-temporal autoregressive model (STVAR) was applied for a very short time scale, 1 min ahead for the first time. From these forecasting model results, a predicted irradiance profile was built. This profile is composed of selected values, spread over one-year prediction data. It shows an important magnitude of irradiance fluctuations. A robust fuzzy MPPT optimization algorithm was applied for a PV system with a capacity of 3 kW peak to overcome this constraint and to estimate the output produced PV power. The fuzzy logic approach has the advantage of improving the transitional regime and reducing fluctuations in the static state whatever changes in the climate there are.

The main novelty of this article is the description and validation of an efficient indirect PV power forecasting method based on short time scale irradiance spatio-temporal forecasting and the MPPT approach. Thus, this work consisted of connecting the contributions of these two fields of research (statistical forecasting irradiance and the MPPT approach). This investigation highlights the results of their combination. The proposed method was applied in a challenging environment, a tropical insular context known by its high solar variability, using in situ real measured solar data. The proposed PV power forecasting method was validated and its performance was very close to that of irradiance forecasting. Efficiency, accuracy, and robustness were studied by simulations for the four seasonal days representing the fast variability of the tropical climate over one year. These results are advantageous to the design and component sizing of PV power plants.

This work is organized as follows. Section 2 (Proposed System Configuration) describes the global structure of the proposed PV system, and its different components: solar PV generator, DC-DC boost converter, and load. In the Section 3 (Solar Forecasting and Control of the Proposed System), the first part describes the used solar forecasting model. After sampling processing, measured and predicted irradiance profiles are given. The second part presents the MPPT fuzzy optimization algorithm. Section 4 (Results and Discussion) shows simulation results obtained for the proposed solution. Finally, the different contributions given in this paper are summarized in the Section 5 (Conclusions).

2. Proposed System Configuration

2.1. Global Structure Design

A block diagram of the proposed control system is shown in Figure 1. The global structure of the studied PV plant is mainly composed of a PV generator (GPV), DC-DC boost converter, and load.
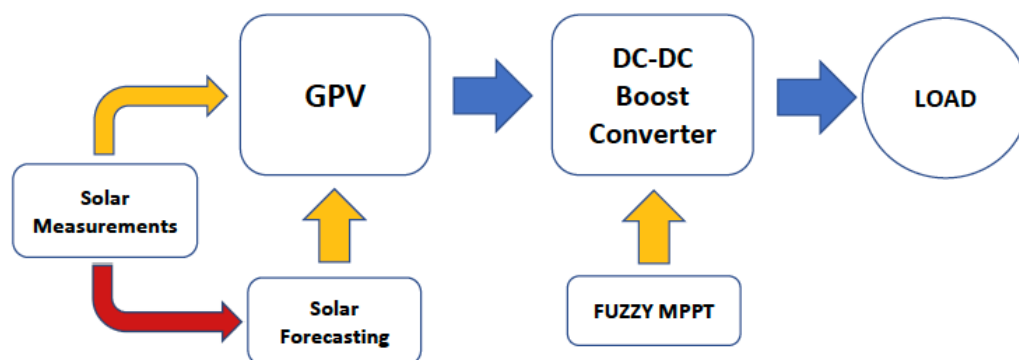

Figure 1. Global structure diagram for PV system.

The description of the proposed structure is as follows:

From solar measurements collected at three sites on Guadeloupe island for a year, and using the STVAR prediction model, we obtained prediction results for a short time scale.

Solar measurements and forecasting data are used to feed our PV production system. For the configuration of our PV system, we propose the use of a DC-DC boost converter, controlled by an MPPT fuzzy LOGIC algorithm to extract the maximum power from the photovoltaic panels.

The objective of this combination is to have an indirect estimate of the power produced by our PV system.

The following sections describe each part of the proposed structure illustrated in Figure 1.

2.2. Solar PV Generator

For more simplicity, photovoltaic cells can be represented using the single-diode model as shown in Figure 2.
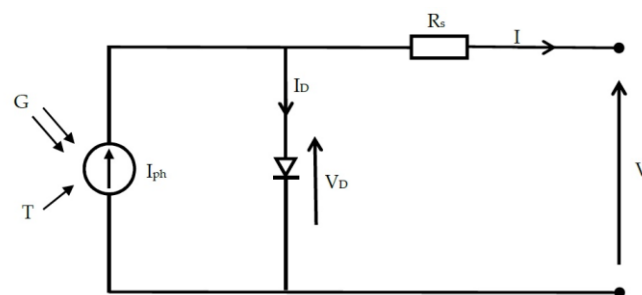

Figure 2. Single-diode model of the PV cell without a shunt resistor.

The series resistance is the internal resistance of the cell, whereby the shunt resistance represents the leakage current of the junction, being generally very large (equivalent to an open circuit), it can be neglected on the equivalent diagram.

The PV cell electrical characteristics are given by the following equations

$$I = I_{ph} - I_D \tag{1}$$

$$I_{ph} = I_{ph}(T_1) \times [1 + K_0 \times (T - T_1)] \tag{2}$$

$$I_{ph}(T_1) = I_{cc}(T_1) \times \left(\frac{G}{G_0}\right) \tag{3}$$

$$K_0 = \frac{I_{cc}(T_2) - I_{cc}(T_1)}{T_2 - T_1} \tag{4}$$

$$I_D = I_s(e^{\left(\frac{V_D}{V_T}\right)} - 1) \tag{5}$$

$$V_T = \frac{nKT}{q} \tag{6}$$

$$V_D = V + R_s I \tag{7}$$

$$R_s = -\frac{dV}{dI_{V_{co}}} - \frac{1}{X_V} \tag{8}$$

$$X_V = \frac{I_s(T_1)}{V_T(T_1)}.e^{\frac{V_{co}(T_1)}{V_T(T_1)}} \tag{9}$$

$$I_s = I_s(T_1) * \left(\frac{T}{T_1}\right)^{3/n} e^{\left(\frac{-q.V_g}{n.K}\right)\left(\frac{1}{T} - \frac{1}{T_1}\right)} \tag{10}$$

$$I_s(T_1) = \frac{I_{cc}(T_1)}{e^{\left(\frac{V_{co}(T_1)}{V_T(T_1)}\right)} - 1} \tag{11}$$

where I, I_{ph}, I_D, I_{cc}, and I_S are, respectively, PV cell output current, photocurrent, diode current, short-circuit current, and saturation current in A. Reference temperature ($T_1 = 25\,°C = 298\,°K$), T: absolute surface temperature, G_0: reference irradiance ($G_0 = 1000\,W/m^2$), K_0: current variation coefficient, q: elementary electron charge, K: Boltzmann's constant, n: diode ideality factor. V_T: thermodynamic potential, V_D: voltage across the diode, V: voltage at the cell terminals, R_s: resistance series, V_{co}: the open circuit voltage.

For solar cell, the equation between current and voltage then becomes

$$I = I_{ph} - I_s \left(e^{\left(\frac{q(V+R_s I)}{nKT} \right)} - 1 \right) \tag{12}$$

The PV generator represents a 3 kW PV module composed of 10 PV modules of 300 Wp (type SunPower SPR-300E-WHT-D) connected in series, and provide 547 V as the output voltage at the maximum power point. The PV panel parameters are given in Appendix A.

2.3. DC-DC Boost Converter

To reduce the number of PV panels used, we chose a boost converter to increase the output voltage of a DC voltage. It ensures the impedance matching between the PV panels and the load. It is composed of the inductor (Lo), input capacitor (Ci), output capacitor (Co), MOSFET transistor switch, and power diode (D). 1 and 2 are terminals for load connection. Figure 3 shows the circuit diagram of the boost converter.
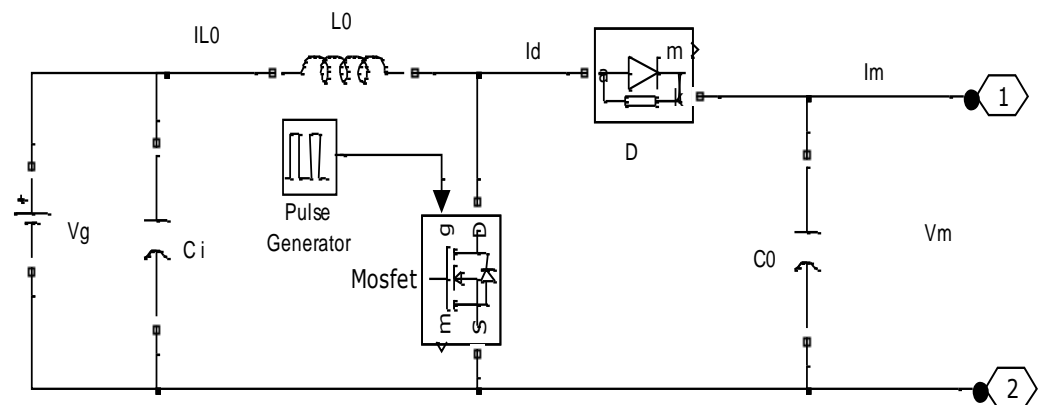

Figure 3. Boost converter circuit.

Equations of the DC-DC converter are given by

$$C_i = \frac{\partial V_g}{\partial t} = I_g - I_{L0} \tag{13}$$

$$L_0 \frac{\partial I_{L0}}{\partial t} = V_g - (1-D)V_m \tag{14}$$

$$L_0 \frac{\partial I_{L0}}{\partial t} = V_g - (1-D)V_m \tag{15}$$

where I_m is the output current of the boost converter (A), I_g is the output current of the PV panels (A), V_m is the output voltage of the boost converter (V), V_g is the output voltage of the PV panels, I_{LO} is the inductor current (A).

The switching state is also governed by a signal of period T and duty cycle D.

3. Solar Forecasting and Control of the Proposed System

3.1. Forecasting Model and Preprocessing of Datasets

3.1.1. Study Context and Experimental Datasets

Experimental measurements were collected on Guadeloupe island; therefore, an insular context located in a tropical climate.

This context favors very frequent cloud formations driven by the diversity of local topography on a small space (orographic clouds) and by synoptic systems due to land/sea contrast [7,8]. This meteorological context leads to the diversity and complexity of solar microclimates. Consequently, the irradiance observed is characterized by high spatial and temporal variability, particularly at short time scales [7,8,62–64]. In this complex context, solar radiation forecasting is challenging, particularly at very short time scales.

The global horizontal irradiance (GHI) was measured at 1 Hz with a pyranometer CM22 from Kipp and Zonen pyranometer (type SP Lite) whose response time is less than a second. The sensor accuracy given by the manufacturer is 3%. For this study we used an averaged database at 1 min of the global horizontal irradiance (GHI) measured for a period starting in January 2012 and ending in December 2012. The measurements were collected at site Petit-canal Gros-cap, along the cliffs (16°38 N, 61°49 W). The forecasting time series at Petit-canal was obtained by the STVAR model using past irradiance observations at the three measurement sites (see Figure 4). Figure 5 displays a five-day irradiance sequence showing high temporal variability. To perform the statistical forecasting model, the temporal trend of the irradiance time series must be removed. Classically, in solar areas, clear sky irradiance is used. This parameter removes the temporal trend of irradiance mainly due to the solar geometry effects by a ratio between the measured irradiance and theoretical clear sky irradiance for the considered 1 min/location.
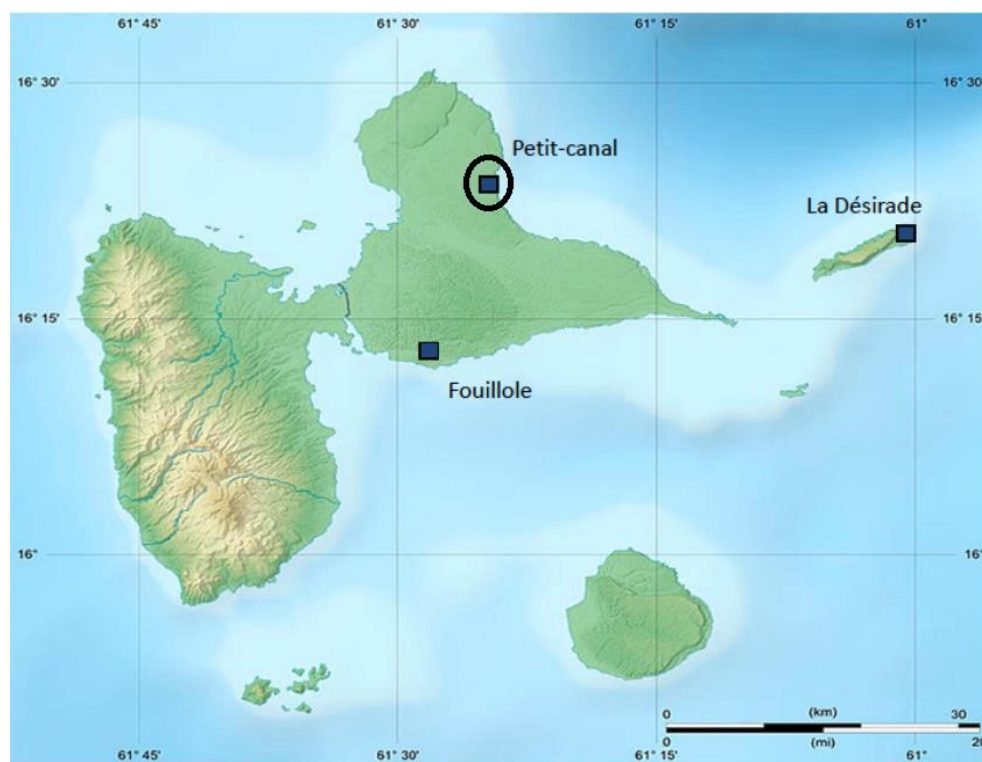

Figure 4. Guadeloupe archipelago and geographical location of three measurement sites: Petit-canal (location of predicted GHI time series selected for our study (black circle)), Fouillole, La Désirade.

3.1.2. Definition of the Forecasting Model: Spatio-Temporal Autoregressive Model—STVAR

The proposed model STVAR (spatio-temporal vector autoregressive) consists of forecasting GHI at a considered location (reference site) by a weighted linear combination of past observations at this location and neighboring locations (spatial predictors) at p lags, plus an error or innovations term, whereas the temporal VAR models uses a linear combination of past observations of *n* variables representing different parameters but located at one site. A spatio-temporal VAR (*p*) process is defined as follows:
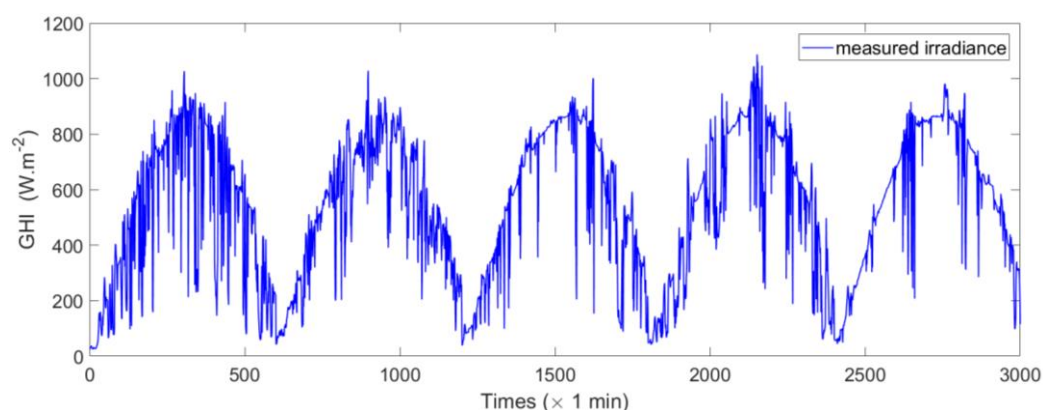
Figure 5. Sequence of five days at 1 min time scale times series of measured ground irradiance GHI.

Consider spatio-temporal variable $Z(s_i, t)$ representing the observations of a stochastic process indexed in $R^2 \times R$. Each observation is made at location s_i and at time t. The considered predictive VAR (vector autoregressive) model (see [22]) is given by

$$Z_t = \sum_{i=1}^{p} R_i(Z_{t-i}) + \varepsilon_t \tag{16}$$

where p is the order corresponding to the time lag; $Z_t = (Z(s_1, t), Z(s_2, t), \ldots, Z(s_N, t))'$ are the spatio-temporal data, ε_t is white noise, and R_i is an $N \times N$ unknown parameter matrix. The N rows of these matrices correspond to the N locations at which time series are observed.

Estimation of the parameters in Equation (16) is obtained with least squares. For more details on the methodology (see Chap. 14 [64]).

If all lagged time series values associated with all measurement sites had to be integrated into the modeling process as input data, the computational process would not be optimized. For more efficiency, a process of the selection of optimal temporal input data (p lags optimal of past observations) and spatial input data (more relevant neighboring sites variable) was developed. This procedure is based on the calculation of the information criterion BIC (Bayesian information criterion) for sequential integration of each spatio-temporal explanatory variable. The relevant spatio-temporal input data are selected by minimization of BIC [6,22]. This procedure is built according to the method proposed in [6,22]. For more details on the modeling process see [6,9].

This process of spatio-temporal input selection was performed on a training dataset. The first month of the dataset was used as a model training dataset and the rest of the year as a test dataset.

STVAR model showed a good predictive performance for a time scale from 5 min to 1 h [6,9]. In this work, this model was performed at 1 min time scale regarding our study context.

3.2. Fuzzy MPPT Algorithm

The studied system is made up of nonlinear elements that need complex and heavy models (photovoltaic panels, electronic power system, etc.). However, most nonlinear control approaches require the availability of a mathematical model of the system. The assured performance is directly related to the accuracy of the model used. That is why we chose to use a fuzzy controller.

To obtain MPP from PV panels, the MPPT algorithm was developed using the fuzzy logic technique [54]. The principle of the MPPT algorithm is to find the maximum point of the curve $P(V)$. For that, we have to bring the error E between dP/dV and its optimal value to zero. When E is positive, the value of P increases, and, conversely, when E is negative,

the value of *P* decreases. For that, a fuzzy logic (FL) controller is used. The classical fuzzy controller diagram is shown in the Figure 6:
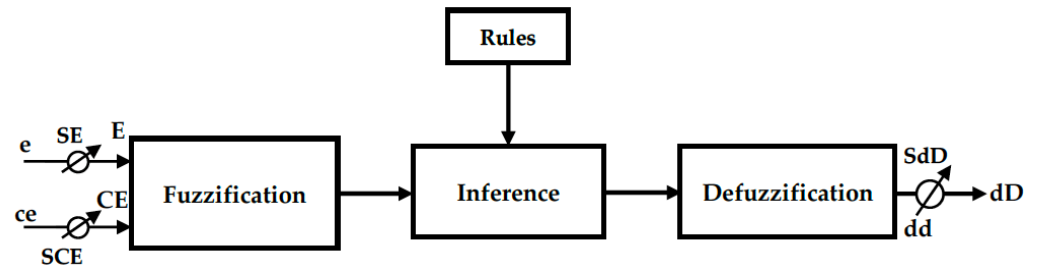

Figure 6. Fuzzy controller general structure.

E: error between *dP/dV* and its optimal value, *CE*: error variation of *E*, *dD*: duty cycle increment. SE, SCE: input gains, SdD: output gain.

1. **Fuzzification and defuzzification** transforms real input variables into fuzzy ones and the reverse. *E* and *CE* are inputs of the FL controller, and *dD* is the output. It represents the variable step of the duty cycle to control the DC-DC converter. The Figure 7 shows the membership functions for *E*, *CE*, and *dD*.
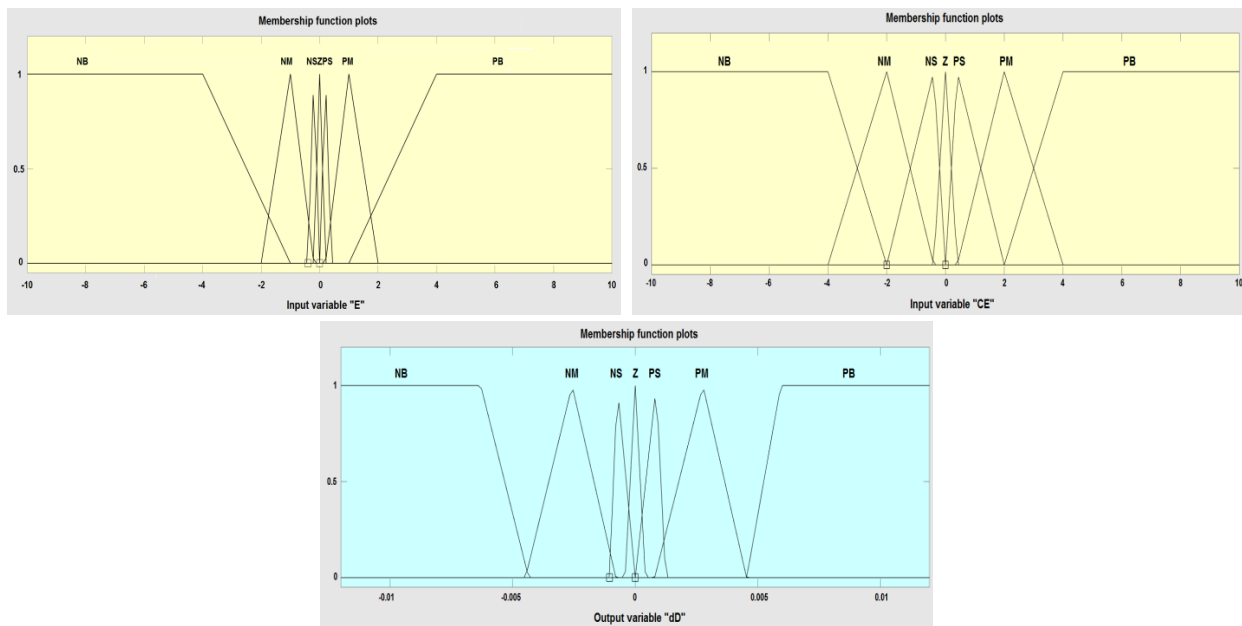

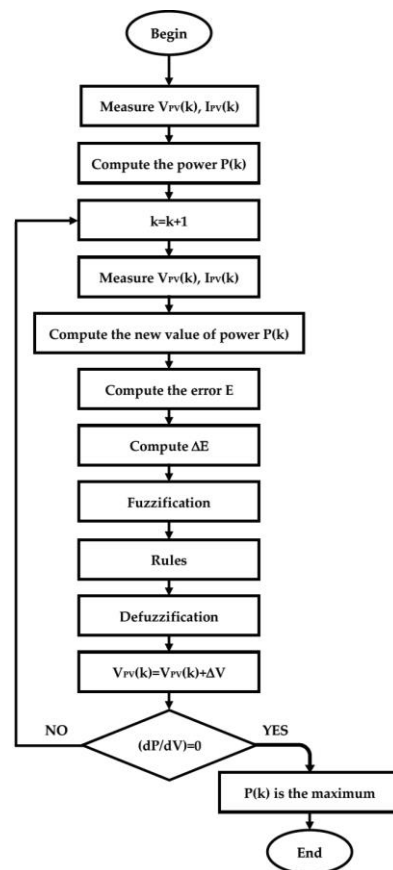**Figure 7.** Membership functions of *E*, *CE*, and *dD*.

Among the different forms of membership functions (trapezoid, Gaussian, and triangular, etc.), the symmetrical triangular form is considered the most appropriate for its simplicity. The use of the nonuniform distributions of fuzzy sets is more suitable for controlling the nonlinear behavior of the PV system. In this study, the symmetrical triangular shape was selected and the boundaries were considered as: [−10, 10] for (*E* and *CE*), and [−0.012, 0.012] for *dD*, respectively.

2. **Inference** is performed using the Mamdani method. Seven linguistic variables are expressed as (NB: negative big), (NM: negative medium), (NS: negative small), (Z: zero), (PS: positive small), (PM: positive medium), (PB: positive big). Table 1 shows the applied rules that ensure the relationship between the inputs and the output of the FL controller. The symmetric rule base is usually used for constant growth systems.

Table 1. Fuzzy rules.

E \ ΔE	NB	NM	NS	Z	PS	PM	PB
NB	NB	NB	NB	NB	NM	NS	Z
NM	NB	NB	NB	NM	NS	Z	PS
NS	NB	NB	NM	NS	Z	PS	PM
Z	NB	NM	NS	Z	PS	PM	PB
PS	NM	NS	Z	PS	PM	PB	PB
PM	NS	Z	PS	PM	PB	PB	PB
PB	Z	PS	PM	PB	PB	PB	PB

The flowchart of the fuzzy controller is shown in the Figure 8.

Figure 8. Fuzzy MPPT technique flowchart.

4. Results and Discussion

4.1. Solar Forecasting Results: Datasets Used for the Simulation

Irradiance in a tropical insular context presents particularly high intraday variability with days that can be clustered as a function of irradiance conditions [10,63,65].

The proposed structure in Figure 1 contains two dynamic systems, operating with two different time scales. The MPPT PV system is very fast (sampling time equal 10^{-4} s) compared with the solar forecasting system (sampling time equal 1 min). For that, the data selection operation is necessary.

A sequence of 11 values was selected with a high magnitude of fluctuations to assess the robustness of the system process. Hence, values of the sequence were chosen according to the high amplitude of fluctuations between two points; that is to say between time t

and t + 1 (1 min). To represent a sequence representative of the high variabilities occurring over the year, a sequence was chosen on a day belonging to a month of a season. One season includes 3 months. Four seasons are considered in an intertropical climate: one dry and sunny season, one rainy and cyclonic season, and two intermediate seasons [8,62,65]. Therefore, four different observations and forecasting days were selected to extract the fluctuation with high amplitude (Figures 9–12). The built sequence is represented in Figure 13. One value was artificially (not consecutive value) chosen to simulate a plateau (see Figure 13, index point of time t_7 and t_8 are not consecutive).
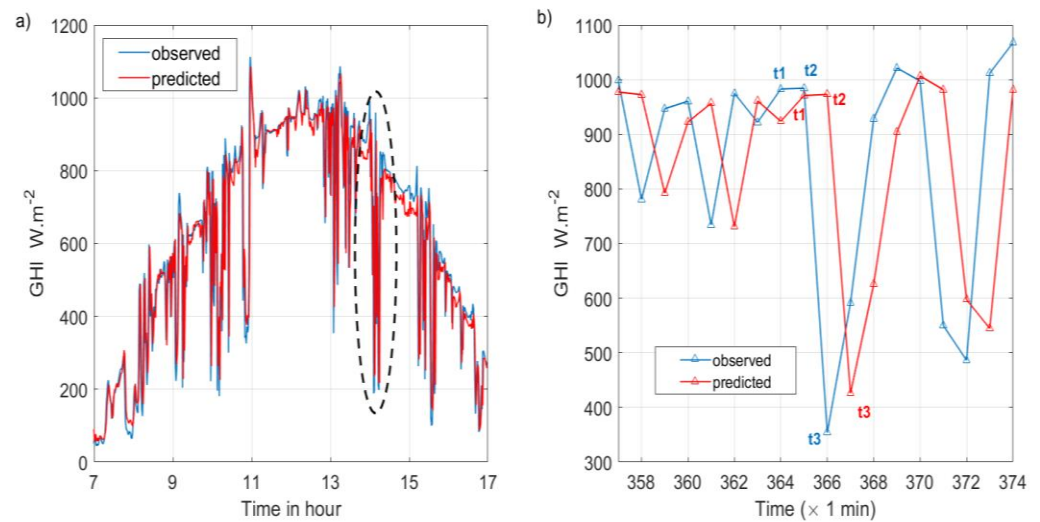

Figure 9. (**a**) Observed signal and predicted signal by STVAR model for a day (5 March). The black dotted-line is the selected part for the zoom. (**b**) Zoom of the part in a black dotted-line ellipse in (**a**).
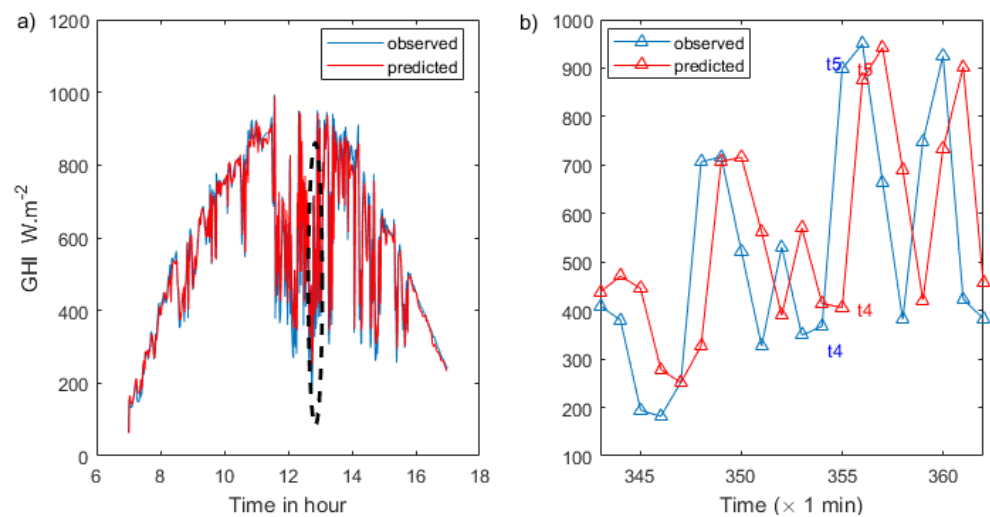

Figure 10. (**a**) Observed signal and predicted signal by STVAR model for a day (11 May). The black dotted-line is the selected part for the zoom. (**b**) Zoom of the part in a black dotted-line ellipse in (**a**).
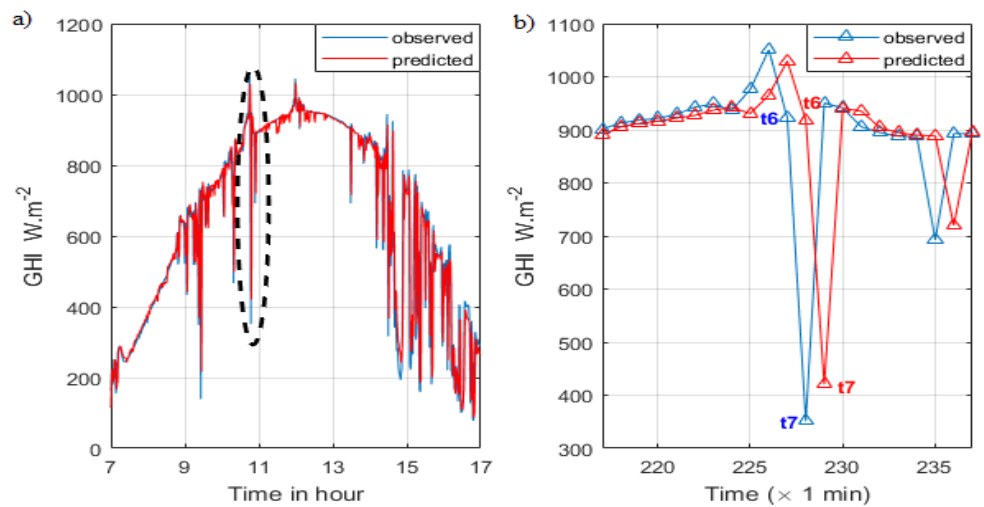
Figure 11. (**a**) Observed signal and predicted signal by STVAR model for a day (29 August). The black dotted-line is the selected part for the zoom. (**b**) Zoom of the part in a black dotted-line ellipse in (**a**).

Figure 12. (**a**) Observed signal and predicted signal by STVAR model for a day (16 December). The black dotted-line is the selected part for the zoom. (**b**) Zoom of the part in a black dotted-line ellipse in (**a**).

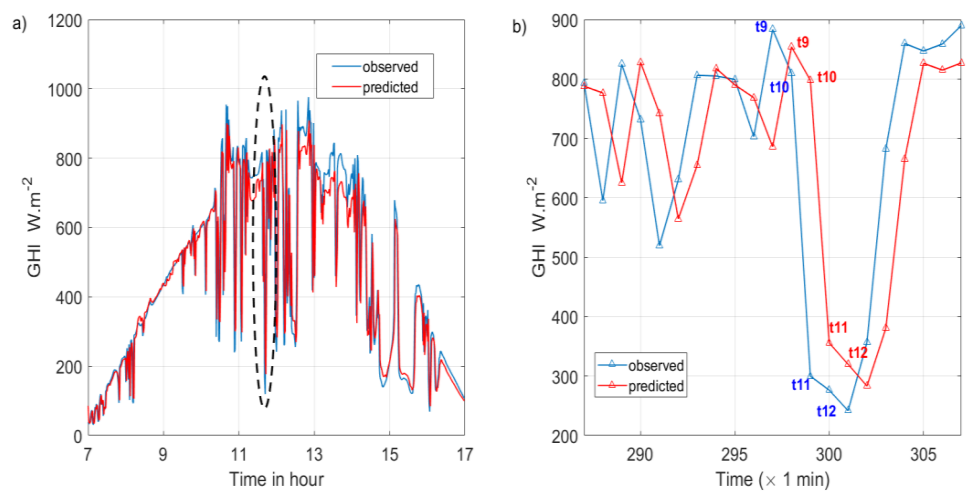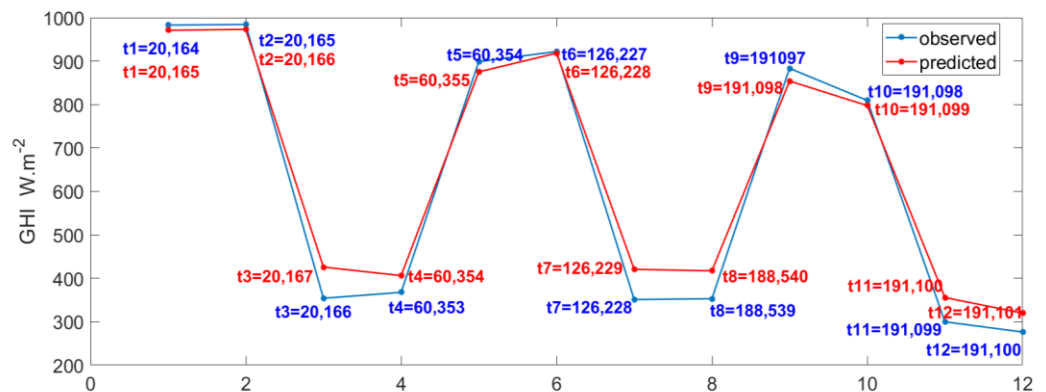**Figure 13.** Sampling of observed and predicted fluctuations irradiance sequence.

There is a time lag between the observations sequence and forecast sequence, which is a particularity of the autoregressive models. This particularity can be observed in

Figures 9b, 10b, 11b and 12b. To build the sequence represented by Figure 13 we removed this time lag.

The values corresponding to time t_i with i from 1 to 3 in the sequence in Figure 9 are indicated.

The values corresponding to time t_i with i from 4 to 5 in the sequence in Figure 10 are indicated.

The values corresponding to time t_i with i varying from 6 to 7 in the sequence in Figure 11 are indicated.

Table 2 gives the solar forecasting performance obtained for 1 min ahead with the STVAR model concerning the four selected days. Model performance is usually assessed by the following statistical metrics: relative Root Mean Squared Error (rRMSE), relative Mean Absolute Error (rMAE), and relative Mean Bias Error (rMBE). Relative error metrics were normalized to the mean observed irradiance data for the considered period.

$$\text{rRMSE} = \frac{\sqrt{\frac{1}{N}\sum\limits_{i=1}^{N}(\widehat{G}-G)^2}}{mean(G)} \times 100\% \tag{17}$$

where $\hat{G}$ is the forecasted values and G the observed values.

$$\text{rMAE} = \frac{\frac{1}{N}\sum\limits_{i=1}^{N}|\hat{G}-G|}{mean(G)} \times 100\% \tag{18}$$

$$\text{rMBE} = \frac{\frac{1}{N}\sum\limits_{i=1}^{N}\widehat{G}-G}{mean(G)} \times 100\% \tag{19}$$

Table 2. Solar forecasting performance for seasonal days.

	Day1 (5 March)	Day2 (11 May)	Day3 (29 August)	Day4 (16 December)
rMAE (%)	11.32	10.82	6.86	13.13
rMBE (%)	−1.65	0.19	−0.03	−2.99
rRMSE (%)	19.99	19.01	14.36	21.80

The values corresponding to time t_i with *i* from 9 to 12 in the sequence in Figure 12 are indicated.

4.2. MPPT Fuzzy Logic Controller Performance

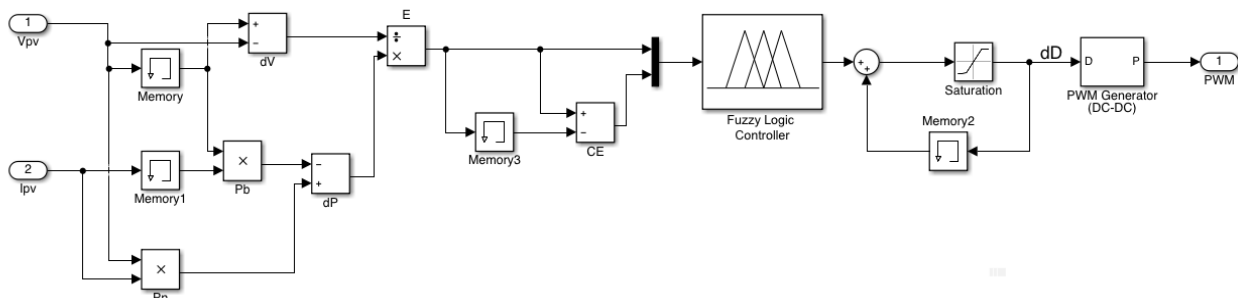Diagram blocks of the fuzzy logic controller are presented in Figure 14:

Figure 14. Diagram blocks of MPPT fuzzy logic controller.

Simulation results are given to check the PV MPPT fuzzy logic performance. The comparison in terms of robustness, rapidity, accuracy, and stability of the proposed con-

troller with the conventional P&O one was tested for a real measured data irradiance profile presented in Figure 15, including sudden changes, which is presented in the solar forecasting section. The temperature was taken as constant and equal at 25 °C.
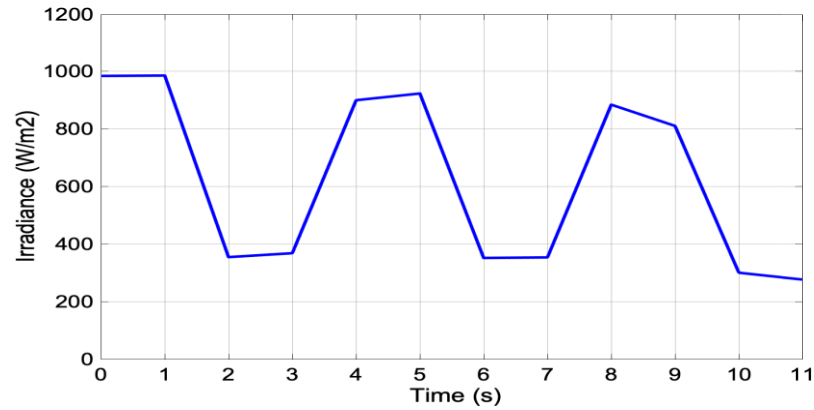

Figure 15. Measured irradiance profile.

Figure 16 shows the dynamic performance of PV voltage, PV current, and output PV power for the two controllers (fuzzy and P&O) under a variable irradiance profile.
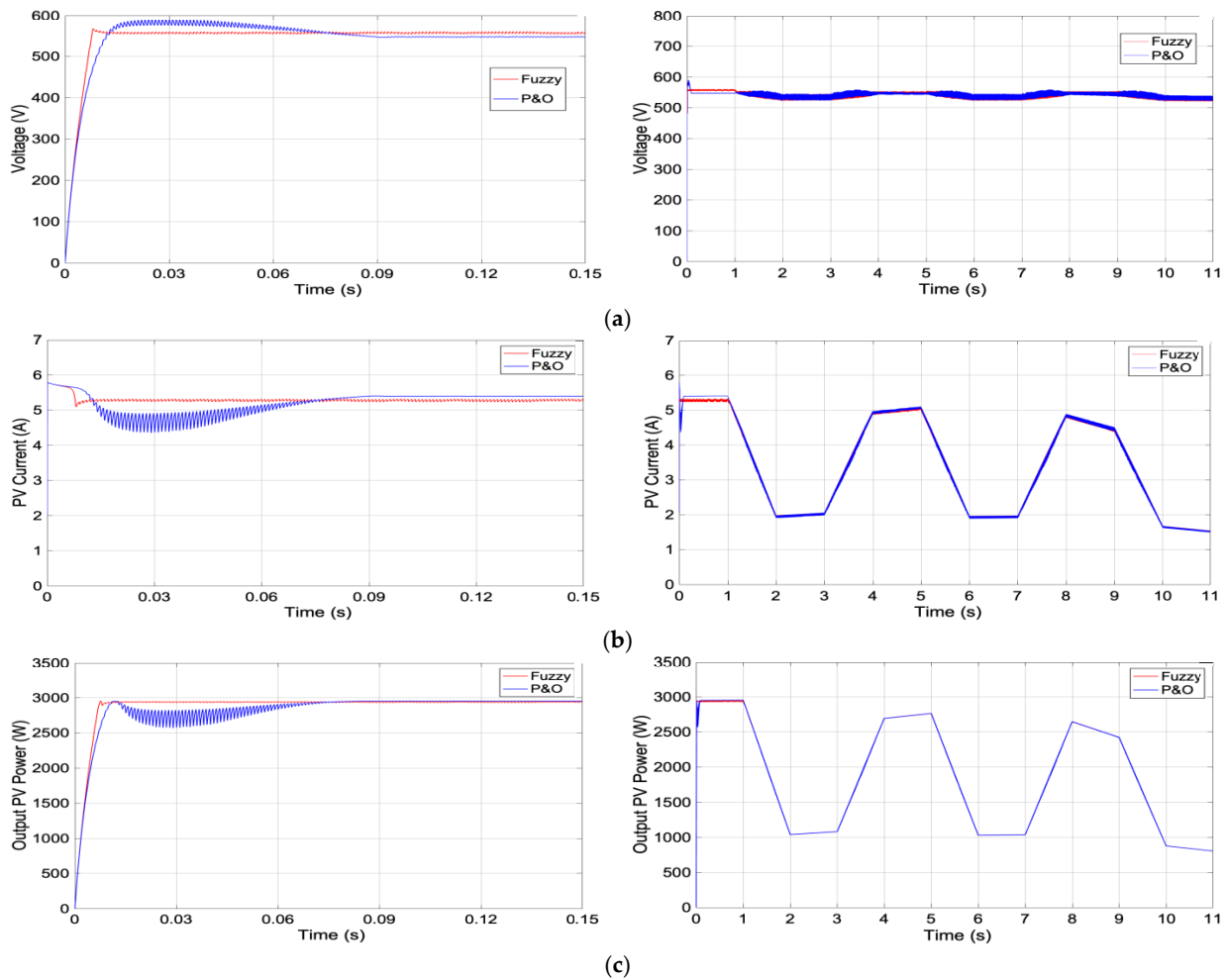

(a)

(b)

(c)

Figure 16. Comparative MPPT PV system performance (fuzzy vs. P&O) for two time scales. (**a**) Output voltage, (**b**) PV current, (**c**) output PV power.

It can be seen that, despite the multiple changes in solar data, the two controllers can follow the change in irradiance to reach the MPP.

The comparison between the two MPPT techniques can be made for performance during the transient and steady state. For that, responses are presented for two time scales. Regarding responses with a short simulation time of 0.15 s, we notice:

- The dynamic response of the P&O controller exhibits unwanted ripples, which are a dangerous drawback for PV systems. In addition, this dynamic response is a pseudo-oscillatory time response with an overshoot equal to 11.87%.
- Compared to P&O, the fuzzy controller converges and reaches the steady state faster with a response time ten times shorter (0.008 s against 0.08 s). We can clearly observe the superiority of the fuzzy controller response in terms of stability and accuracy with respect to the P&O one, which is less stable with ripples and oscillation, and less accurate with a slight permanent steady-state error.

Simulation results demonstrate very clearly that the proposed scheme (fuzzy MPPT controller) exhibits a fast and accurate dynamic response and stable steady-state output power against a rapid change in the irradiance profile.

4.3. Output PV Power Prediction

The PV power generation plant of 3 kW controlled by the MPPT fuzzy logic technique was fed with the measured and predicted solar data results given in Section 4.1. The solar measurements were collected from the Petit-canal site in Guadeloupe. Predicted solar data were obtained using the STVAR model for a very short time scale of 1 min ahead. Four seasonal days, representing the fast variability of a tropical climate over 10 h of sunshine every day, were selected. The produced output power of the PV system was calculated using measured and predicted data in the cases of the four seasonal days.

In order to evaluate the accuracy and efficiency of the PV power prediction, *rRMSE*, *rMAE*, and *rMBE* were calculated for the four seasonal days. The results are given in Table 3.

Table 3. PV power prediction performance for seasonal days.

	Day 1	Day 2	Day 3	Day 4
rMAE (%)	11.58	11.09	6.99	13.70
rMBE (%)	−1.60	0.19	−0.03	−3.14
rRMSE (%)	20.43	19.46	14.65	22.60

From the simulation results given in Figure 17 and Table 3 for the same four days in Section 4.1 belonging to different seasons, we notice that:

- Output PV power variability calculated from predicted data in the cases of the four days is close to that calculated from the measured one, which demonstrates the efficiency of the proposed method.
- The influence of intraday variability on the predictive performance of the model is also observed. The highest errors are obtained for day 4 corresponding to the day presenting the highest intraday variability (*rRMSE* = 22.60%, *rMAE* = 13.70%), whereas the lowest errors are obtained for day 3 presenting the lowest intraday variability and with less pronounced variation (*rRMSE* = 14.65%, *rMAE* = 6.99%). Consequently, the results are an illustration of the predictive performance model as a function of the irradiance conditions as seen in the results in the literature [7,9,66].
- According to the *rMBE* results, the model tends to underestimate the observed values (negative values of *rMBE*).
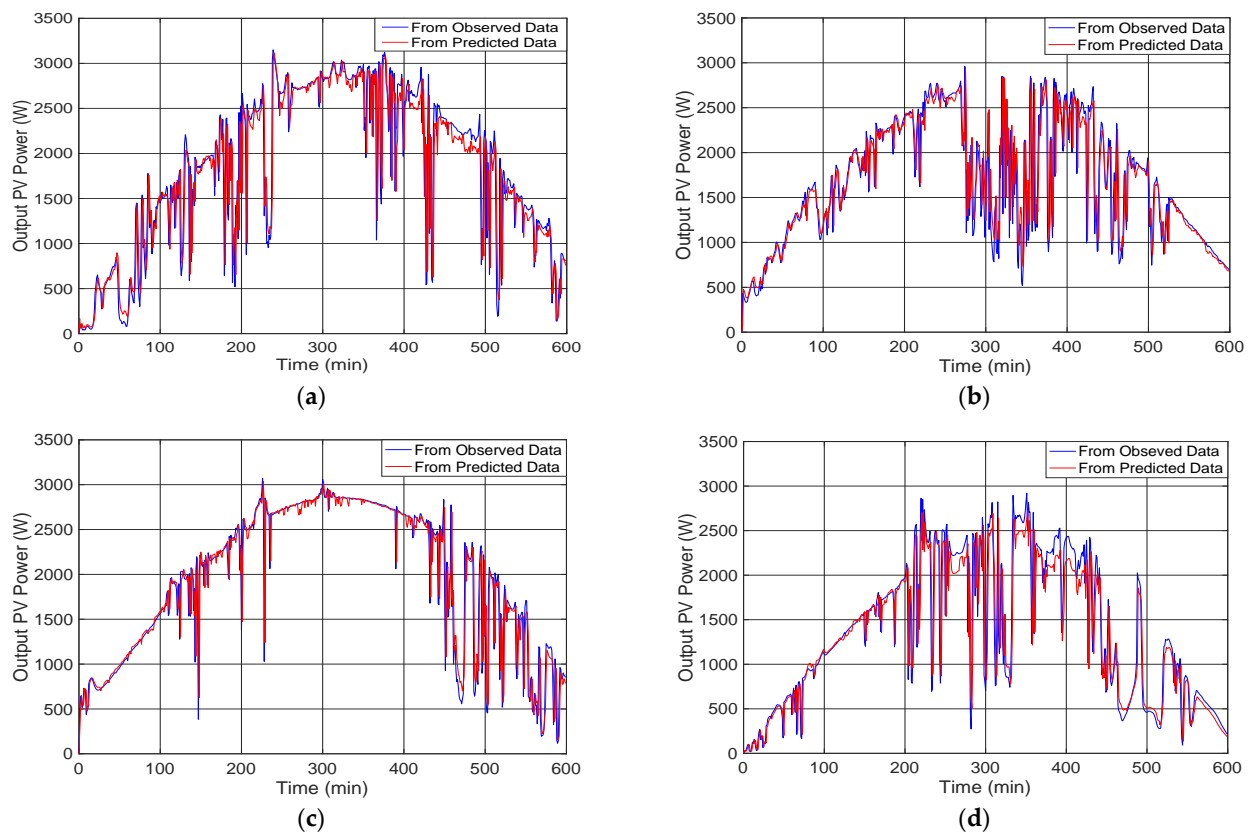
Figure 17. Output PV power prediction over 4 season days (1 min ahead). (**a**) Day1 (5 March); (**b**) Day2 (11 May); (**c**) Day3 (29 August); (**d**) Day4 (16 December).

Consequently, by comparison of the solar irradiance prediction previously mentioned in Figures 9–12 and Table 2 with the indirect output power prediction given in Figure 17 and Table 3, the output PV power model has the same predictive performance trend as the irradiance forecasting model (STVAR).

$$\text{skill} - \text{score} = (1 - \frac{RMSE_{model}}{RMSE_{persistence}}) \times 100 \tag{20}$$

Skill-score is an error metric that compares the model performance with a reference model described by Equation (20). According to [67], the skill parameter (skill-score) proposed is a comparison with the proposed model and the persistence model. Persistence forecasts, as the name implies, are defined as having the output PV power that persists for the next time step. It is a naive model often used as a reference forecasting model. Table 4 presents the results of the skill-score for the same 4 days as in Table 3. A positive skill-score significates that the proposed model has a better predictive performance than the persistence model. A negative skill-score shows that the proposed model has a lower predictive performance than the persistence model.

Table 4. PV power prediction skill-score performance for seasonal days.

	Day1 (5 March)	Day2 (11 May)	Day3 (29 August)	Day4 (16 December)
rRMSE (%) Persistence model	21.33	20.24	15.50	22.87
Skill-score (%)	4.22	3.85	6.71	1.18

Consequently, Table 4 exhibits a better predictive performance of our forecasting technic than the persistence model whatever the seasonal day. This metric error is also able to compare if our approach could be useful to other researchers.

5. Conclusions

The existence of a sudden and rapid change in the meteorological conditions, especially in a tropical context, led us to propose through the present work a robust and reliable solution based on real measured and predicted irradiance data. The proposed work deals with an indirect PV power production prediction of a PV power generation plant for a short time scale. The PV power generation plant is composed of 10 solar panels (3 kW) and a DC-DC boost converter. The PV power prediction approach is based on a combination of solar forecasting results and a fuzzy MPPT technique. Solar measurements data were collected on Guadeloupe Island.

Solar forecasting using the STVAR model, applied for the first time at 1 min time scales, allowed us to obtain a representative irradiance profile to test the efficiency of the proposed MPPT PV solution. The latter is designed to face two challenges: maximum power extraction from the PV generator, and output PV power prediction. The fuzzy MPPT technique ensures a better optimization performance presenting good robustness with respect to extreme climatic conditions. The output PV power prediction performance depends on the used solar prediction method, the MPPT PV technique, and irradiance profile variability. The same predictive performance trend of the output PV power model as the irradiance forecasting model (STVAR) is an expected result due to the structure of the PV system. Indeed, the structure combines the irradiance forecasting model and the forecasting PV output model. The strength and limits of the irradiance forecasting model (STVAR model) are consequently imposed on the final results (output PV forecasting); hence, the importance of an appropriate choice of forecasting irradiance model. The investigation of a new global structure diagram for a PV system integrating two approaches (statistical forecasting irradiance and an MPPT approach) showed the strengths and limitations of this system. In a subsequent investigation, we will test another forecasting model that has already shown good predictive performance in the literature, at this very short time scale (1 min). Operationally, such an approach would mesh with operational industry-targeted forecast services.

Author Contributions: Conceptualization, F.M.; Data curation, M.A.; Formal analysis, R.C.; Investigation, M.A.; Methodology, F.M.; Project administration, F.M.; Software, F.M.; Supervision, R.C.; Validation, F.M.; Visualization, R.C.; Writing—original draft, F.M. and M.A. All authors have read and agreed to the published version of the manuscript.

Conflicts of Interest: The authors declare no conflict of interest.

Appendix A

We chose model SunPower SPR-300E-WHT-D. This panel is composed of 96 cells series-connected ($n_s = 96$).

- These data represent the typical performance of the panel SPR-300E, which is measured with output, and no additional equipment effect is included such as the diodes and the cables. The data are based on the measures under the standard conditions SRC (Standard Reporting Conditions, knowledge also: STC or Standard Test Conditions), which set:
- an Irradiance of 1 kW/m^2 (1 sun) to a spectrum AM 1.5;
- a temperature of the cell of 25 °C.

Table A1. Photovoltaic panel parameters.

Maximal power	P_m	300 W
Voltage for maximal power	V_{pm}	54.7 V
Current for maximal power	I_{pm}	5.49 A
Current of short circuit	I_{sc}	5.87 A
Voltage of open circuit	V_{oc}	64 V
Temperature coefficient of I_{sc}	T_{sc}	(0.061738) %/°C
Temperature coefficient of V_{oc}	T_{oc}	(−0.2727) %/°C

References

1. Gioutsos, D.M.; Blok, K.; van Velzen, L.; Moorman, S. Cost-optimal electricity systems with increasing renewable energy penetration for islands across the globe. *Appl. Energy* **2018**, *226*, 437–449. [CrossRef]
2. Silsirivanich, N. Fluctuation Characteristics effect analysis of Solar Irradiance Data by Wavelet transform. *Energy Procedia* **2017**, *138*, 301–306. [CrossRef]
3. Zafeiropoulou, M.; Mentis, I.; Sijakovic, N.; Terzic, A.; Fotis, G.; Maris, T.I.; Vita, V.; Zoulias, E.; Ristic, V.; Ekonomou, L. Forecasting Transmission and Distribution System Flexibility Needs for Severe Weather Condition Resilience and Outage Management. *Appl. Sci.* **2022**, *12*, 7334. [CrossRef]
4. Sijakovic, N.; Terzic, A.; Fotis, G.; Mentis, I.; Zafeiropoulou, M.; Maris, T.I.; Zoulias, E.; Elias, C.; Ristic, V.; Vita, V. Active System Management Approach for Flexibility Services to the Greek Transmission and Distribution System. *Energies* **2022**, *15*, 6134. [CrossRef]
5. Calif, R.; Schmitt, F.G.; Huang, Y.; Soubdhan, T. Intermittency study of high frequency global solar radiation sequences under a tropical climate. *Sol. Energy* **2013**, *98*, 349–365. [CrossRef]
6. André, M.; Dabo-Niang, S.; Soubdhan, T.; Ould-Baba, H. Predictive spatio-temporal model for spatially sparse global solar radiation data. *Energy* **2016**, *111*, 599–608. [CrossRef]
7. Lauret, P.; Voyant, C.; Soubdhan, T.; David, M.; Poggi, P. A benchmarking of machine learning techniques for solar radiation forecasting in an insular context. *Sol. Energy* **2015**, *112*, 446–457. [CrossRef]
8. Cécé, R.; Bernard, D.; Brioude, J.; Zahibo, N. Microscale anthropogenic pollution modelling in a small tropical island during weak trade winds: Lagrangian particle dispersion simulations using real nested LES meteorological fields. *Atmos. Environ.* **2016**, *139*, 98–112. [CrossRef]
9. André, M.; Perez, R.; Soubdhan, T.; Schlemmer, J.; Calif, R.; Monjoly, S. Preliminary assessment of two spatio-temporal forecasting technics for hourly satellite-derived irradiance in a complex meteorological context. *Sol. Energy* **2019**, *177*, 703–712. [CrossRef]
10. Soubdhan, T.; Emilion, R.; Calif, R. Classification of daily solar radiation distributions using a mixture of Dirichlet distributions. *Sol. Energy* **2009**, *83*, 1056–1063. [CrossRef]
11. Monjoly, S.; André, M.; Calif, R.; Soubdhan, T. Forecast Horizon and Solar Variability Influences on the Performances of Multiscale Hybrid Forecast Model. *Energies* **2019**, *12*, 2264. [CrossRef]
12. Stein, J.S.; Hansen, C.W.; Reno, M.J. The variability index: A new and novel metric for quantifying irradiance and PV output variability. In Proceedings of the World Renewable Energy Forum, Denver, CO, USA, 13–17 May 2012; pp. 13–17.
13. Lenox, C.; Nelson, L. Variability comparison of large-scale photovoltaic systems across diverse geographic climates. In Proceedings of the 25th European Photovoltaic Solar Energy Conference, Valencia, Spain, 6–10 September 2010.
14. Van Haaren, R.; Morjaria, M.; Fthenakis, V. Empirical assessment of short-term variability from utility-scale solar PV plants. *Prog. Photovolt. Res. Appl.* **2012**, *22*, 548–559. [CrossRef]
15. Lave, M.; Reno, M.J.; Broderick, R.J. Characterizing local high-frequency solar variability and its impact to distribution studies. *Sol. Energy* **2015**, *118*, 327–337. [CrossRef]
16. Perez, R.; David, M.; Hoff, T.E.; Jamaly, M.; Kivalov, S.; Kleissl, J.; Lauret, P.; Perez, M. Spatial and Temporal Variability of Solar Energy. *Found. TrendsR Renew. Energy* **2016**, *1*, 1–44. [CrossRef]
17. Kleissl, J. *Solar Energy Forecasting and Resource Assessment*; Academic Press: Cambridge, MA, USA, 2013.
18. Finkenstadt, B.; Held, L.; Isham, V. *Statistical Methods for Spatio-Temporal Systems*; CRC Press: Boca Raton, FL, USA, 2006.
19. Cressie, N.; Johannesson, G. Fixed rank Kriging for very large data sets. *J. R. Stat. Soc. Ser. B* **2008**, *70*, 209–226. [CrossRef]
20. Cressie, N.; Wikle, C.K. *Statistics for Spatio-Temporal Data*; John Wiley & Sons: Hoboken, NJ, USA, 2011.
21. Cellura, M.; Cirrincione, G.; Marvuglia, A.; Miraoui, A. Wind speed spatial estimation for energy planning in Sicily: A neural kriging application. *Renew. Energy* **2008**, *33*, 1251–1266. [CrossRef]
22. De Luna, X.; Genton, M.G. Predictive spatio-temporal models for spatially sparse enviromental data. *Stat. Sin.* **2005**, *15*, 547–568.
23. Liu, H.; Shi, J.; Erdem, E. Prediction of wind speed time series using modified Taylor Kriging method. The 3rd International Conference on Sustainable Energy and Environmental Protection, SEEP. *Energy* **2010**, *35*, 4870–4879. [CrossRef]
24. Porcu, E.; Mateu, J.; Saura, F. New classes of covariance and spectral density functions for spatio-temporal modelling. *Stoch. Environ. Res. Risk Assess.* **2008**, *22*, 65–79. [CrossRef]

25. Inoue, T.; Sasaki, T.; Washio, T. Spatio-Temporal Kriging of Solar Radiation Incorporating Direction and Speed of Cloud Movement. 2012. Available online: https://www.jstage.jst.go.jp/article/pjsai/JSAI2012/0/JSAI2012_1K2IOS1b3/_article/-char/ja/ (accessed on 25 August 2022).

26. Yang, D.; Gu, C.; Dong, Z.; Jirutitijaroen, P.; Chen, N.; Walsh, W.M. Solar irradiance forecasting using spatial-temporal covariance structures and time-forward kriging. *Renew. Energy* **2013**, *60*, 235–245. [CrossRef]

27. Yang, D.; Dong, Z.; Reindl, T.; Jirutitijaroen, P.; Walsh, W.M. Solar irradiance forecasting using spatio-temporal empirical kriging and vector autoregressive models with parameter shrinkage. *Sol. Energy* **2014**, *103*, 550–562. [CrossRef]

28. Aryaputera, A.W.; Yang, D.; Zhao, L.; Walsh, W.M. Very short-term irradiance forecasting at unobserved locations using spatio-temporal kriging. *Sol. Energy* **2015**, *122*, 1266–1278. [CrossRef]

29. Yang, D.; Ye, Z.; Lim, L.H.I.; Dong, Z. Very short term irradiance forecasting using the lasso. *Sol. Energy* **2015**, *114*, 314–326. [CrossRef]

30. Glasbey, A.; Allcroft, C.D. A spatiotemporal autoregressive moving average model for solar radiation. *J. R. Stat. Soc. Ser. C* **2008**, *57*, 343–355. [CrossRef]

31. Dambreville, R.; Blanc, P.; Chanussot, J.; Boldo, D. Very short-term forecasting of the Global Horizontal Irradiance using a spatio-temporal autoregressive model. *Renew. Energy* **2014**, *72*, 291–300. [CrossRef]

32. Ahmed, R.; Sreeram, V.; Mishra, Y.; Arif, M.D. A review and evaluation of the state-of-the-art in PV solar power forecasting: Techniques and optimization. *Renew. Sustain. Energy Rev.* **2020**, *124*, 109792. [CrossRef]

33. Rajagukguk, R.A.; Ramadhan, R.A.A.; Lee, H.-J. A Review on Deep Learning Models for Forecasting Time Series Data of Solar Irradiance and Photovoltaic Power. *Energies* **2020**, *13*, 6623. [CrossRef]

34. Lappalainen, K.; Wang, G.C.; Kleissl, J. Estimation of the largest expected photovoltaic power ramp rates. *Appl. Energy* **2020**, *278*, 115636. [CrossRef]

35. Husein, M.; Chung, I.-Y. Day-Ahead Solar Irradiance Forecasting for Microgrids Using a Long Short-Term Memory Recurrent Neural Network: A Deep Learning Approach. *Energies* **2019**, *12*, 1856. [CrossRef]

36. Das, U.K.; Tey, K.S.; Seyedmahmoudian, M.; Mekhilef, S.; Idris, M.Y.I.; van Deventer, W.; Horan, B.; Stojcevski, A. Forecasting of photovoltaic power generation and model optimization: A review. *Renew. Sustain. Energy Rev.* **2018**, *81*, 912–928. [CrossRef]

37. Sobri, S.; Koohi-Kamali, S.; Rahim, N.A. Solar photovoltaic generation forecasting methods: A review. *Energy Convers. Manag.* **2018**, *156*, 459–497. [CrossRef]

38. Raza, M.Q.; Nadarajah, M.; Ekanayake, C. On recent advances in PV output power forecast. *Sol. Energy* **2016**, *136*, 125–144. [CrossRef]

39. Radicioni, M.; Lucaferri, V.; De Lia, F.; Laudani, A.; Lo Presti, R.; Lozito, G.M.; Riganti Fulginei, F.; Schioppo, R.; Tucci, M. Power Forecasting of a Photovoltaic Plant Located in ENEA Casaccia Research Center. *Energies* **2021**, *14*, 707. [CrossRef]

40. Yu, D.; Choi, W.; Kim, M.; Liu, L. Forecasting Day-Ahead Hourly Photovoltaic Power Generation Using Convolutional Self-Attention Based Long Short-Term Memory. *Energies* **2020**, *13*, 4017. [CrossRef]

41. Niccolai, A.; Dolara, A.; Ogliari, E. Hybrid PV Power Forecasting Methods: A Comparison of Different Approaches. *Energies* **2021**, *14*, 451. [CrossRef]

42. Marcos, J.; Marroyo, L.; Lorenzo, E.; Alvira, D.; Izco, E. Power output fluctuations in large scale PV plants: One year observations with one second resolution and a derived analytic model. *Prog. Photovolt. Res. Appl.* **2011**, *19*, 218–227. [CrossRef]

43. Mills, A.; Ahlstrom, M.; Brower, M.; Ellis, A.; George, R.; Hoff, T.; Kroposki, B.; Lenox, C.; Nicholas, M.; Stein, J.; et al. *Understanding Variability and Uncertainty of Photovoltaics for Integration with the Electric Power System*; Lawrence Berkeley National Lab.(LBNL): Berkeley, CA, USA, 2009; Volume 9. [CrossRef]

44. Nasir, M.; Khan, H.A.; Khan, I.; Hassan, N.U.; Zaffar, N.A.; Mehmood, A.; Sauter, T.; Muyeen, S.M. Grid Load Reduction through Optimized PV Power Utilization in Intermittent Grids Using a Low-Cost Hardware Platform. *Energies* **2019**, *12*, 1764. [CrossRef]

45. Andrean, V.; Chang, P.C.; Lian, K.L. A Review and New Problems Discovery of Four Simple Decentralized Maximum Power Point Tracking Algorithms—Perturb and Observe, Incremental Conductance, Golden Section Search, and Newton's Quadratic Interpolation. *Energies* **2018**, *11*, 2966. [CrossRef]

46. Ali, A.; Almutairi, K.; Malik, M.Z.; Irshad, K.; Tirth, V.; Algarni, S.; Zahir, M.H.; Islam, S.; Shafiullah, M.; Shukla, N.K. Review of Online and Soft Computing Maximum Power Point Tracking Techniques under Non-Uniform Solar Irradiation Conditions. *Energies* **2020**, *13*, 3256. [CrossRef]

47. Karami, N.; Moubayed, N.; Outbib, R. General review and classification of different MPPT Techniques. *Renew. Sustain. Energy Rev.* **2017**, *68*, 1–18. [CrossRef]

48. Motahhir, S.; El Hammoumi, A.; El Ghzizal, A. The most used MPPT algorithms: Review and the suitable low-cost embedded board for each algorithm. *J. Clean. Prod.* **2020**, *246*, 118983. [CrossRef]

49. Zhu, Y.; Kim, M.K.; Wen, H. Simulation and Analysis of Perturbation and Observation-Based Self-Adaptable Step Size Maximum Power Point Tracking Strategy with Low Power Loss for Photovoltaics. *Energies* **2019**, *12*, 92. [CrossRef]

50. Li, C.; Chen, Y.; Zhou, D.; Liu, J.; Zeng, J. A High-Performance Adaptive Incremental Conductance MPPT Algorithm for Photovoltaic Systems. *Energies* **2016**, *9*, 288. [CrossRef]

51. Chalh, A.; El Hammoumi, A.; Motahhir, S.; El Ghzizal, A.; Subramaniam, U.; Derouich, A. Trusted Simulation Using Proteus Model for a PV System: Test Case of an Improved HC MPPT Algorithm. *Energies* **2020**, *13*, 1943. [CrossRef]

52. Alshareef, M.; Lin, Z.; Ma, M.; Cao, W. Accelerated Particle Swarm Optimization for Photovoltaic Maximum Power Point Tracking under Partial Shading Conditions. *Energies* **2019**, *12*, 623. [CrossRef]
53. Hadji, S.; Gaubert, J.-P.; Krim, F. Real-Time Genetic Algorithms-Based MPPT: Study and Comparison (Theoretical an Experimental) with Conventional Methods. *Energies* **2018**, *11*, 459. [CrossRef]
54. Robles Algarín, C.; Taborda Giraldo, J.; Rodríguez Álvarez, O. Fuzzy Logic Based MPPT Controller for a PV System. *Energies* **2017**, *10*, 2036. [CrossRef]
55. Chang, S.; Wang, Q.; Hu, H.; Ding, Z.; Guo, H. An NNwC MPPT-Based Energy Supply Solution for Sensor Nodes in Buildings and Its Feasibility Study. *Energies* **2019**, *12*, 101. [CrossRef]
56. Ahmed, S.; Muhammad Adil, H.M.; Ahmad, I.; Azeem, M.K.; e Huma, Z.; Abbas Khan, S. Supertwisting Sliding Mode Algorithm Based Nonlinear MPPT Control for a Solar PV System with Artificial Neural Networks Based Reference Generation. *Energies* **2020**, *13*, 3695. [CrossRef]
57. Ali, K.; Khan, L.; Khan, Q.; Ullah, S.; Ahmad, S.; Mumtaz, S.; Karam, F.W.; Naghmash. Robust Integral Backstepping Based Nonlinear MPPT Control for a PV System. *Energies* **2019**, *12*, 3180. [CrossRef]
58. Kececioglu, O.F.; Gani, A.; Sekkeli, M. Design and Hardware Implementation Based on Hybrid Structure for MPPT of PV System Using an Interval Type-2 TSK Fuzzy Logic Controller. *Energies* **2020**, *13*, 1842. [CrossRef]
59. Zadeh, L. Fuzzy sets. *Inf. Control.* **1965**, *8*, 338–353. [CrossRef]
60. Tchoketch Kebir, G.F.; Larbes, C.; Ilinca, A.; Obeidi, T.; Tchoketch Kebir, S. Study of the Intelligent Behavior of a Maximum Photovoltaic Energy Tracking Fuzzy Controller. *Energies* **2018**, *11*, 3263. [CrossRef]
61. Hassan, T.-U.; Abbassi, R.; Jerbi, H.; Mehmood, K.; Tahir, M.F.; Cheema, K.M.; Elavarasan, R.M.; Ali, F.; Khan, I.A. A Novel Algorithm for MPPT of an Isolated PV System Using Push Pull Converter with Fuzzy Logic Controller. *Energies* **2020**, *13*, 4007. [CrossRef]
62. Badosa, J.; Haeffelin, M.; Chepfer, H. Scales of spatial and temporal variation of solar irradiance on Reunion tropical island. *Sol. Energy* **2013**, *88*, 42–56. [CrossRef]
63. Voyant, C.; Soubdhan, T.; Lauret, P.; David, M.; Muselli, M. Statistical parameters as a means to a priori assess the accuracy of solar forecasting models. *Energy* **2015**, *90*, 671–679. [CrossRef]
64. Pena, D.; Tiao, G.C.; Tsay, R.S. *A Course in Time Series Analysis*; John Wiley & Sons: Hoboken, NJ, USA, 2001.
65. Soubdhan, T.; Abadi, M.; Emilion, R. Time dependent classification of solar radiation sequences using best information criterion. *Energy Procedia* **2014**, *57*, 1309–1316. [CrossRef]
66. Monjoly, S.; André, M.; Calif, R.; Soubdhan, T. Hourly forecasting of global solar radiation based on multiscale decomposition methods: A hybrid approach. *Energy* **2017**, *119*, 288–298. [CrossRef]
67. Coimbra, C.F.M.; Kleissl, J.; Marquez, R. Overview of solar forecasting method and a metric for accuracy evaluation. In *Solar Energy Forecasting and Resource Assessment*; Kleissl, J., Ed.; Elsevier: Amsterdam, The Netherlands, 2013; pp. 171–194.